MODELLING OF BOILING IN DIFFUSION ABSORPTION REFRIGERATORS FOR CFD ANALYSES

Nina Penkova, Yordan Stoyanov, Kalin Krumov, Ivan Kassabov,
Vesselin Iliev, Liliana Zashcova, Darina Dimitrova

University of Chemical Technology and Metallurgy, 8 Kliment Ohridski Blvd.
Sofia 1797, Bulgaria, nina@uctm.edu (N.P.); j.stoianov@uctm.edu (Y.S.);
kkrumov@uctm.edu (K.K.); ivankassabov@mail.bg (I.K.);
veso@uctm.edu (V.I.); zashcova@mail.bg (L.Z.); daritodim@gmail.com (D.D.).

Received 03 July 2026
Accepted 18 September 2026 *DOI: 10.59957/jctm.v61.i6.2026.17*

ABSTRACT

The evaporation of binary mixtures is a complex transport phenomenon, including fluid flow, heat exchange, mass transfer and phase change in multi-component, multi-phase domain. The boiling and buoyancy of the vapor bubbles in the generators of absorption diffusion refrigerators (DAR) lead to the bubble pump effect, which is the main driving force of the absorption cycle. Computational fluid dynamics (CFD) is an advanced approaches to improve the efficiency of DAR's components. Its implementation for the boiling process requires modelling of the thermodynamical processes of the binary mixtures, which is also open problem, especially at vertical generators with rectifier for separation of the saturated liquid and steam, and absorbent recirculation. This paper presents a conception for CFD simulation of binary mixture boiling in such generators, including a new be-temperature model of the saturation temperature. The models are tested based on an experimentally obtained diffusion absorption cycle of ammonia-water solution and its application is confirmed.

Keywords: binary mixtures, boiling, diffusion absorption refrigerator, CFD, saturation temperature, be-temperature model.

INTRODUCTION

Diffusion-absorption refrigerators were developed nearly 200 years ago by Baltzar von Platen and Carl Münters during their studies at the Royal Institute of Technology in Stockholm [1]. The silent operation, lack of moving parts and ability to be driven by electrical and thermal energy are advantages that have made DAR subjects of continuous research and development [2 - 4]. The working fluid of this type of system is a binary solution of a low-boiling-point refrigerant and a higher-boiling-point absorbent, which makes the thermodynamic processes in the system complex to understand, model and design. For this reason, the modern market lacks diffusion absorption refrigerators with cooling capacities above 100 W. According to Bisulandu et al., the application of CFD analyses in the absorbers and desorbers (generators) of DAR is an essential tool for developing and optimizing these systems [4]. The authors highlight that CFD studies must be aimed to generators as key elements of the absorption technologies.

Models and numerical studies of the binary mixture processes in the generator of DAR are known from the literature [5 - 10]. Some of them are focused on the heat transfer in the units [6 - 8]. Others were carried out by numerical solving the partial differential equations describing the fluid flow processes at boiling [9, 10]. A complex model and CFD simulations of binary mixture boiling in vertical generators with recirculation of the poor of refrigerant absorbent, taking into account the changeable saturation temperature with the refrigerant concentration have not been reported to now.

An approach for CFD analysis of the Multiphysics processes during the boiling of ammonia-water solution in such generators, including a new be-temperature

mathematical model of the saturation temperature are developed and presented in this paper. The application of the model to express the saturation temperature as function of the ammonia concentration and wet vapour quality at experimentally obtained absorption cycle of a laboratory DAR is demonstrated.

EXPERIMENTAL

Absorption cycle of DAR

A simplified scheme of a laboratory DAR, made by Edibon, is presented on Fig. 1. It is a typical variant of DAR with vertical generators. A separate scheme of the coupled generator, heat exchanger and their geometries without the thermal insulation are shown on Fig. 2.

An electrical heater with a rated power of 120 W is the heat source in thermal contact to the external metal wall of the generator (Fig. 2a). A gas burner is an additional option for energy supply.

The ammonia-rich solution in State 4 inflows in the "pipe in pipe" heat exchanger (State 1o), absorbs thermal energy and boils to State of wet vapour 2o. This vapour is consisted of saturated steam (State 2") and saturated liquid (State 2'), separated by a porous rectifier on the generator outlet. The steam bubbles, formed during the boiling, rise, generating a thermosiphon (bubble pump) effect, which moves the solution through the elements of the refrigerator. The liquid in State 2' flows down to the heat exchanger, where it exchanges heat with the ammonia-rich solution. The poor of ammonia liquid, cooled to State 3, enters the absorber and absorbs the ammonia vapour.

The ammonia-rich saturated steam (State 2") enters the condenser, where the ammonia condenses at constant pressure p_c, releasing a heat flow to the room environment. The subcooled ammonia-rich liquid after the condenser is throttled from State 5o to State 6o of wet vapour. This two-phase mixture with reduced pressure p_e enters the evaporator and subsequently evaporates to the State 7o in a freezing chamber, and superheats to State 8o in a cooling chamber. After mixing with the non-condensed vapour (5'), the ammonia rich vapour enters the absorber, where it is absorbed by the ammonia-poor liquid, releasing the heat of absorption to the environment.

Sensors ST1 - ST10 measure important temperatures of the binary solution and the subsequent environments, ensuring enough information to fix the absorption cycle of DAR [12].

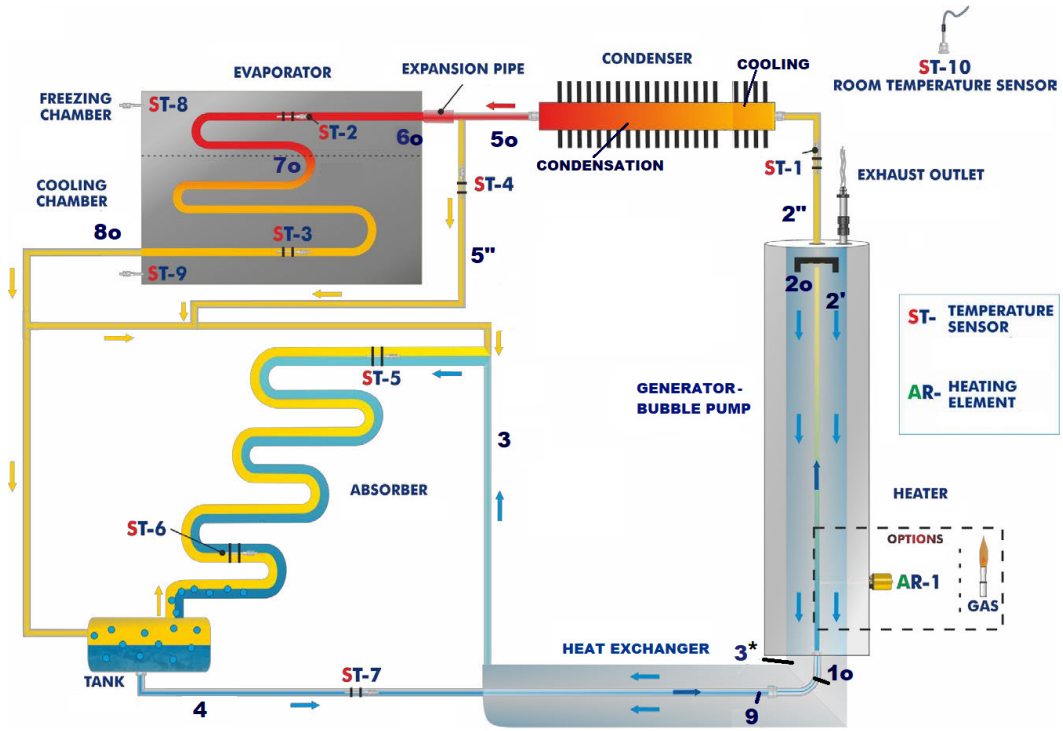
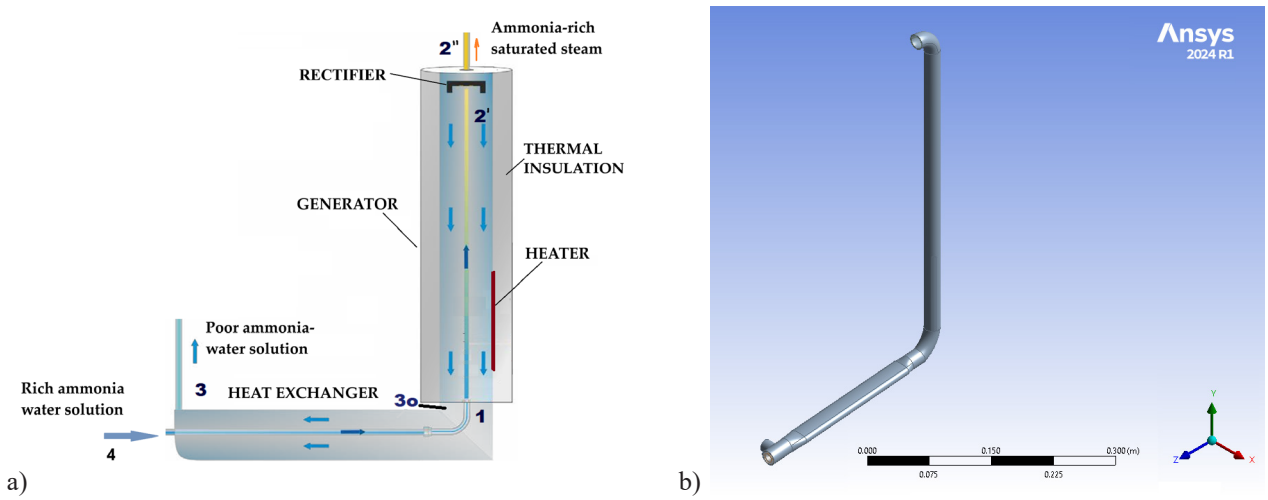


Fig. 1. Scheme of laboratory diffusion absorption refrigeration system TRAB [11, 12].



a) b)

Fig. 2. Coupled generator and heat exchanger. Scheme (a) and geometrical model (b).

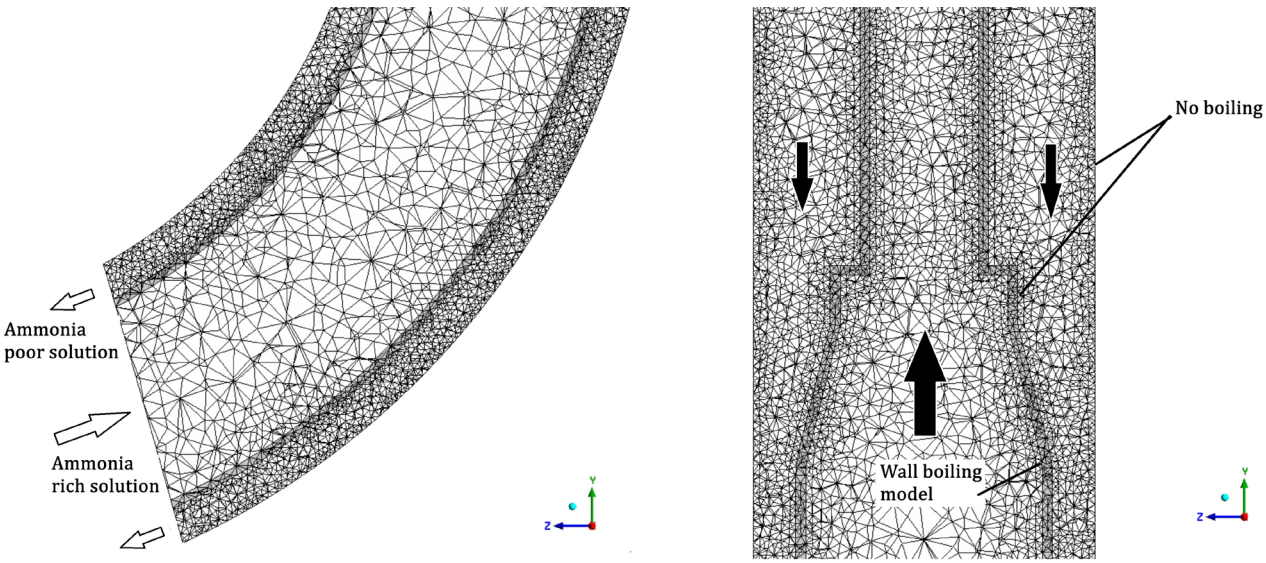


Fig. 3. Parts of the finite element mesh.

CFD models of the boiling and bubble pump effect in DAR.

A three-dimensional geometrical model of a coupled generator and "pipe in pipe" heat exchanger, including the heat exchanging metal walls is generated and discretized by finite element mesh. The mesh must be enough fine to allow proper computation of the two-phase domain of the boiling binary mixture in the regions of boiling (Fig. 3). The thermal insulation, external walls and the electrical heater can be excluded by the geometrical model and can be modelled via the boundary conditions for faster numerical solution. The rectifier can be modelled by a porous domain with porosity, obtained by its volume and mass.

The binary mixture in the states, described above, may include four components: liquid and steam ammonia and water with mass fractions α_i:

$$\sum_{i=1}^{4} \alpha_i = 1 \qquad (1)$$

The governing system, solved numerically by Finite Volume Method, includes the partial differential equations below [13]. The equations and methods for their solution are well known, so their description is concise, except for terms, related to the modelling of the boiling.

Continuity equation

$$\frac{1}{\rho_i}\left[\frac{\partial(\alpha_i\rho_i)}{\partial t}+\nabla.(\alpha_i\rho_i\vec{u}_i)=\sum_{i=1}^{n}(\dot{m}_i)\right] \quad (2)$$

where ϱ_i are the densities of the components, kg m^{-3}; $\vec{u}_i$ *is the* velocity vectors on the different axes, m s^{-1}; $\dot{m}_i$ is the mass flow sources, kg s^{-1}:

$$\dot{m}_i=\frac{q_e}{r+c_p\max(0,T_s-T_L)} \quad (3)$$

In Eq. (3) q_e is the heat flux, released at a condensation or absorbed at evaporation, W m^{-2}; r = specific heat for the phase change, J kg^{-1}, c_p = specific heat capacity, J kg^{-1} K^{-1}, T_s – saturation temperature, K; T_L = liquid temperature, K.

Models of the saturation temperature are suggested below.

Momentum equations

$$\frac{\partial(\alpha_i\rho_i\vec{u}_i)}{\partial_t}+\nabla(\alpha_i\rho_i\vec{u}_i\vec{u}_l)=-\nabla p+\nabla(\mu_e\nabla\vec{u}_l)+$$
$$+\alpha_i\rho_i\vec{g}+\vec{F} \quad (4)$$

where g = gravity acceleration, m s^{-1}; p = pressure, Pa μ_e = effective dynamic viscosity (sum of the molecular and turbulent ones), Pa s.

The total interfacial momentum exchange force acting on a dispersed phase (such as bubbles) inside a continuous fluid phase, includes several components:

$$F=F_D+F_L+F_{TD} \quad (5)$$

where F_D = drag force, opposing the relative motion between the dispersed particles and the surrounding fluid. For bubbles with diameter d_G it is:

$$F_D=-\frac{3}{4d_G}C_D\rho_L\alpha_G|u_G-u_L|(u_G-u_L) \quad (6)$$

The dimensionless drag coefficient C_D can be computed by Reynolds number *Re*:

$$C_D=\frac{24}{Re}(1+0.1Re^{0.75}) \quad (7)$$

The lift force F_L and the turbulent dispersion force F_{TD} are:

$$F_L=C_L\rho_L\alpha_G(u_G-u_L)rot(u_L) \quad (8)$$

$$F_{TD}-\frac{3}{4}C_D\frac{\alpha_L}{d_G}|u_G-u_L|\frac{v_{EL}}{\sigma_{VD}}\left(\frac{1}{\alpha_L}+\frac{1}{\alpha_G}\right)\nabla\alpha_G \quad (9)$$

In (9) v_{el} and σ_{VD} are respectively the effective kinematic viscosity of the liquid and Prandtl number (usually 0.9). The indexes "*L*" and "*G*" are denoted to liquid and vapour parameters.

Energy equation

$$\frac{\partial\rho_i h_i}{\partial t}+\nabla(\alpha_i u_i h_i)=\nabla\left(\alpha_i(-\lambda_e\nabla T)\right)+\frac{\alpha_i}{\rho_i}\frac{\partial P}{\partial t}+$$
$$+\frac{\alpha_i}{\rho_i}u_i\nabla P-\frac{\Gamma_i h_i}{\rho_i}+\frac{q_w A_w}{\rho_i} \quad (10)$$

where h_i = specific enthalpies of the components, J kg^{-1}; λ_e = effective thermal conductivity (sum of molecular and turbulent ones), W m^{-1} K^{-1}; Γ_i = mass source per unit volume, kg m^{-3} s^{-1}; q_w = wall heat flux, W m^{-2}, A_w = area, m^2.

Turbulence model

The practice shows that Shere Stress Transport (SST) and k-ε model work well at the investigated case [13]. The two equations of k-ε model are:

$$\frac{\partial}{\partial t}(\rho k)+\frac{\partial}{\partial x_i}(\rho k u_i)=\frac{\partial}{\partial x_j}\left[\left(\mu+\frac{\mu_t}{\sigma_k}\right)\frac{\partial k}{\partial x_j}\right]+$$
$$+G_k+G_b-\rho\varepsilon-Y_M+S_K \quad (11a)$$

$$\frac{\partial}{\partial t}(\rho\varepsilon)+\frac{\partial}{\partial x_i}(\rho\varepsilon u_i)=\frac{\partial}{\partial x_i}\left[\left(\mu+\frac{\mu_t}{\sigma_\varepsilon}\right)\frac{\partial\varepsilon}{\partial x_j}\right]+$$
$$+G_{1\varepsilon}\frac{\varepsilon}{K}(G_k+C_{3\varepsilon}G_b)-C_{2\varepsilon}\rho\frac{\varepsilon^2}{k}+S_\varepsilon \quad (11b)$$

where k = turbulence kinetic energy J kg^{-1}; ε = turbulence kinetic energy dissipation rate W kg^{-1}; μ_t = turbulent dynamic viscosity (eddy viscosity), Pa s; G = generated mass flux, kg s^{-1} m^{-2}; S = additional source, kg s^{-1} m^{-2}.

$Y_m=2\varrho\varepsilon M_t^2$, where M_t is turbulent Max number. The indexes *"k"* and *"b"* are denoted to flow and buoyancy. The constant in the equations above are calibrated for each case [13].

Rensselaer Polytechnic Institute (RPI) Wall boiling model

According to PRI Wall boiling model the total heat flux q_w, supplied by a heated wall is partitioned into three

distinct heat transfer mechanisms [14]:

$$q_w = q_c + q_q + q_e \quad (12)$$

where q_c = convective heat flux, q_q = quenching heat flux, transferred to the cold bulk liquid that rushes in to fill the void space when a bubble detaches from the wall; q_e = evaporative heat flux, W m^{-2}. They are computed by the following ways:

$$q_c = (1 - A_w) h_c (T_w - T_L) \quad (13)$$

$$h_c = \frac{\rho C_p u_\tau}{T^+} \quad (14)$$

$$q_q = A_w h_q (T_w - T_L) \quad (15)$$

$$A_w = \pi \left(a \frac{d_W}{2} \right)^2 N \quad (16)$$

$$h_q = \frac{2}{\sqrt{\pi}} f \sqrt{t_{wait} k_L \rho_L C_{PL}} \quad (17)$$

$$t_{wait} = \frac{0.8}{f} \quad (18)$$

$$q_e = \dot{m}_w h_{LG} \quad (19)$$

$$h_{LG} = \frac{k_L}{d_G} Nu \quad (20)$$

$$d_G = \frac{d_{G,1}(T_{sub} - T_{sub,2}) + d_{G,2}(T_{sub} - T_{sub,1})}{T_{sub,2} - T_{sub,1}} \quad (21)$$

$$Nu = 2 + 0.6 Re^{1/2} Pr^{1/3} \quad (22)$$

$$\dot{m}_w = \rho_G \frac{\pi}{6} d_w^3 f N \quad (23)$$

$$d_W = d_{ref} e^{-\frac{T_s - T_L}{\Delta T_{refd}}} \quad (24)$$

$$N = N_{ref} = \left(\frac{T_W - T_L}{\Delta T_{refN}} \right)^P \quad (25)$$

In the equations above A_w = area of influence (fraction of the wall where the boiling occurs); h_c = convection heat transfer coefficient, W m^{-2} K^{-1}; h_q = quenching heat transfer coefficient, W m^{-2} K^{-1} h_{LG} = heat transfer coefficient at boiling/condensation, W m^{-2} K^{-1}; N = active nucleation site density, m^{-2}; f = bubble departure frequency, s^{-1}; t_{wait} = period of bubble waiting time, calculated from the bubble detachment frequency, s; d_G = bubbles diameter, m; Nu = Nuselt number. The indexes *"w"*, *"ref"* and *"sub"* are denoted respectively to parameters near the wall, referent parameters and subcooled liquid.

Volume of fluid (VOF) algorithm

VOF is used to compute the volume fraction of the steam and liquid in the elements of the mech, formed by the buoyancy [13]. It is supposed that there exists a free surface between the liquid and the vapour fraction. In practice it is negligible in the narrow space in the generator. That also impose a fine elements mesh.

Modelling of the saturation temperature of the binary mixture

The Wall-boiling model above cannot be applied directly for the binary liquid solutions, as they are pure liquid like with changeable saturation temperature during the boiling. To address this problem, an approach for modelling the relation between the saturation temperature, ammonia concentration and subsequent quality of the wet vapour of the boiling binary mixture in vertical generators of DAR is developed in this section.

In principle, T_s of the depends on the pressure and refrigerant concentration. The pressure in the generator is nearly constant [4, 5]. Therefore, T_s can be expressed as a function of the refrigerant concentration, which decrease during the boiling with the increasing of the quality X of the wet vapour at the established pressure (Fig. 3). These dependencies can be developed based on Patek and Klomfar functions for predicting vapor-liquid equilibrium conditions of boiling ammonia-water solution [15]:

Saturated liquid - bubble - point

$$T_b(\mathrm{p,x}) = T_o \sum_j a_i (1 - x)^{m_i} \left[ln \left(\frac{p_o}{p} \right) \right]^{n_i}, \mathrm{K} \quad (26)$$

Saturated vapour (dew - point)

$$T_d(\mathrm{p,y}) = T_o \sum_j a_i (1 - y)^{m_i} \left[ln \left(\frac{p_o}{p} \right) \right]^{n_i}, \mathrm{K} \quad (27)$$

where: T_b(p,x) = bubble-point temperature (saturated liquid) K; T_d (p,y) = dew-point temperature (saturated vapour), K; x = ammonia mole fraction in liquid phase; y = ammonia mole fraction in vapor phase; p = pressure (MPa); T_0 = 100 K; p_0 = 2 MPa.

The coefficients a_i, m_i and n_i in (26) and (27) are available in table mode in [15]. Knowing the pressure during the boiling, the temperatures of the saturated liquid and vapour can be expressed as functions of the

ammonia concentrations in the saturated liquid ξ′ and saturated vapour ξ″.

$$T_b = T_b(\xi'), K \quad (28)$$
$$T_d = T_d(\xi''), K \quad (29)$$

The inverse functions of (28) and (29) gives the dependencies of the ammonia concentrations in the saturated liquid and vapour:

$$\xi' = \xi'(T_b) = \xi'(T_s) \quad (30)$$
$$\xi'' = \xi''(T_b) = \xi''(T_s) \quad (31)$$

ξ_{rich}e boiling starts at initial ammonia concentrationn on the generator inlet (State 4 on Fig. 1 and Fig. 2). The mass balance during the process is:

$$\dot{m}_{rich} = \dot{m}_i' + \dot{m}_v'' \quad (32)$$

where $\dot{m}_{rich}$, $\dot{m}_i'$ and $\dot{m}_v''$ respectively are the mass flows of the ammonia-rich solution on the generator inlet, ammonia-poor saturated liquid and ammonia-rich saturated vapour, obtained at the boiling.

Therefore, the quality X of the wet vapour of the binary mixture is:

$$X = \frac{\dot{m}_v''}{\dot{m}_l' + \dot{m}_v''} = \frac{\dot{m}_v''}{\dot{m}_{rich}} = \frac{\xi_{rich} - \xi'}{\xi'' - \xi'} \quad (33)$$

Considering (30) and (31), X can be expressed by the saturation temperature T_S:

$$X = \frac{\xi_{rich} - \xi'(T_s)}{\xi''(T_s) - \xi'(T_s)} \quad (34)$$

The inverse function of (34) is a polynomial-like dependency between the saturation temperature and the quality X of the wet vapour:

$$T_s = T_s(X) \quad (35)$$

When the volume fractions of the saturated liquid and steam are computed via VOF algorithm during the iterative solution of the mathematical model above, the quality X, which is a mass fraction on the saturated vapour in the finite elements, can be computed by "If-Then-Else" logical function:

$$X = \begin{cases} 0 \ at \ Vv = 0 \\ \frac{V_v \cdot \rho_v''}{V_v \cdot \rho_v' + (1 - V_v) \cdot \rho_l''} \ at \ Vv < 1 \\ 1 \ at \ Vv = 1 \end{cases} \quad (36)$$

where V_v= vapour volume fraction, ρ_v' and ρ_i'' are the densities of the saturated vapour and saturated liquid, kg m^{-3}.

It is assumed that the ammonia-poor solution, moving downwards in the generator, does not boil, since its saturation temperature is higher than the temperature at the top point. The lack of boiling in this liquid is modelled by assuming high (non-real) saturation temperatures in the nodes with velocity vectors, directed downwards. For velocity vectors in the upward direction, the boiling temperature is determined by (35). This dependency is like the bi-viscous model, used in CFD to approximate ideal Bingham plastics. It is also computed by a conditional operator of the If-Then-Else type. In the case where the upward direction coincides with the direction of the y-axis in a Cartesian coordinate system and V is the projection of the velocity vector on this axis, the be-temperature model is:

$$T_s = \begin{cases} T_s = T_s(X), K \ at \ V > 0 \ m \ s^{-1} \\ 1000000 \ K \ at \ V < 0 \ m \ s^{-1} \end{cases} \quad (37)$$

Boundary conditions

Conditions of the boundaries of the coupled generator and pipe-in-pipe heat exchanger for the solution of the equations above are summarized in Table 1.

Physical conditions

Modelling of the vapour and liquid properties of the binary mixture as functions of the refrigerant concentration is possible using well known dependencies or library of specialised software [13, 17]. Taking into account the complex models, the iterative solution for four-component media is slow even at large capacity hardware. To simplify the numerical computations, especially the Wall boiling model, the liquid solution can be modelled as a pure fluid. The vapour (steam) is a mixture of two real gases with properties, strongly depending on the pressure and the temperature. Given

Table 1. Boundary conditions.

Boundary	Boundary conditions
Ammonia-rich liquid inlet (State 4)	Fixed mass flow and temperature, obtained at absorption cycle analysis
Ammonia-poor liquid outlet (State 2")	Opening boundary at opening pressure = p_c
Ammonia-rich steam outlet	Opening boundary at opening pressure = p_c
Electrical heater contact	Heat flux: $\dot{q} = (P / A)$, W m^{-2} P = electrical power, W; A=contact surface, m^2.
Insulated external surfaces	Heat transfer through multilayer insulation wall at heat flux $\dot{q} = f_1(T_a)$, W m^{-2} T_a = ambient temperature, K
Non-insulated external surfaces	Heat transfer through metal wall at heat flux $\dot{q} = f_2(T_a)$, W m^{-2}
Fluid/solid interface - internal pipe surfaces	Wall boiling model
Fluid/solid interface -external surfaces of the internal pipe	Non activated Wall boiling model

that the molar masses of the ammonia and water vapor differ by 6 % and the higher concentration of the easily boiling ammonia in the vapor mixture (Table 2), the gas mixture can be modelled as real ammonia gas with an accuracy of less than 3 %. The enthalpies of the liquid and vapour mixture can be computed via the enthalpy's functions according to Patek and Klomfar in order to achieve proper heat of phase change in the Wall-boiling model above [15].

Transient analyses

Experimental observations show that a stable operating mode of the DAR is obtained at least 20 minutes after switching on the power supply. Therefore, it is necessary to solve the system of equations using a transient algorithm at small time steps and initial conditions as close as possible to the observed states for the numerical simulation of the established processes. Another option is to use a pseudo-transient steady-state algorithm, also starting from the initial conditions [13].

RESULTS AND DISCUSSION

The be-temperature model is applied to fix the dependencies of (37) at an experimentally obtained diffusion absorption cycle of the laboratory unit at maximal power input (P = 109 W).

The "captured" parameters of the binary mixture of the boundaries of the geometrical model on Fig. 2, obtained by measurements and calculations according to Todorov and Daskalov, are summarised in Table 2 [18, 19].

The computed saturation temperatures of the bubble-point (saturated liquid) and dew-point (saturated vapor) according to equations (26) and (27) at the established pressure in the generator (14.2 Bar) are given in table 3.

The curves of the saturated states are presented in T - ζ diagram on Fig. 4. The heating of the binary mixture in the heat exchanger of the laboratory DAR is illustrated by process 4 - 1o. The established experimentally boiling process proceeds between State 1o ($\zeta_{rich} = 0.45$) and State 2o.

The functions (30) and (31), obtained by the information in Table 2 are visualized on Fig. 5.

The saturation temperature at the boiling along the generator varies within the range 83ºC - 140ºC. The concentration of the ammonia-poor solution decreases from 0.45 to 0.2 during this process.

The changes in temperatures, concentrations and quality X in the possible interval of boiling at initial ammonia concentration $\zeta_{rich} = 0.45$ are presented in Table 3 and Fig. 6. The last two columns of the table are used to derive the saturation temperature function of pressure in equations (35) and (37).

Table 2. Parameters of ammonia-water mixtures on the boundaries.

Inlet of the pipe-in-pipe heat exchanger (State 4)		
Ammonia concentration, ξ_{rich}	kg kg^{-1}	0.45
Pressure, p_e	Bar	3.32
Temperature, t_4	°C	30.5
Specific enthalpy, h_4	kJ kg^{-1}	50
Ammonia mass flow	kg s^{-1}	0.058
Water mass flow	kg s^{-1}	0.071
Mixture mass flow, $\dot{m}_{rich}$	kg s^{-1}	0.129
Cross-section area	m^2	7.84E-05
Velocity	m s^{-1}	1.641
Saturated steam after the rectifier (State 2")		
Ammonia concentration, $\xi_{2"}$	kg kg^{-1}	0.9
Pressure, p_c	Bar	14.2
Temperature, t_2	°C	139.8
Specific enthalpy, $h_{2"}$	kJ kg^{-1}	530
Mass flow of the evaporated ammonia	kg s^{-1}	0.057
Mass flow of the evaporated water	kg s^{-1}	0.006
Mass flow of the vapour mixture, $\dot{m}_v''$	kg s^{-1}	0.064
Saturated liquid on the outlet of the pipe-in-pipe heat exchanger (State 3)		
Ammonia concentration, ξ_3	kg kg^{-1}	0.2
Pressure, p_c	Bar	14.2
Temperature, t_3	°C	35.9
Specific enthalpy, h_3	kJ kg^{-1}	80
Mass flow of the liquid boundary solution, $\dot{m}_i'$	kg s^{-1}	0.065
Ammonia mass flow	kg s^{-1}	0.001
Water mass flow	kg s^{-1}	0.064
Cross section area	m^2	0.0001534
Velocity	m s^{-1}	0.420

Table 3. Saturation temperatures of the saturated liquid and vapour as function of the molar (x) and mass fractions (ζ) of the ammonia.

x	0	0.11	0.21	0.31	0.41	0.51	0.61	0.71	0.81	0.91	1.00
$\zeta'=\zeta''$	0	0.10	0.20	0.30	0.40	0.50	0.60	0.70	0.80	0.90	1.00
t_b, ºC	196.2	165.4	139.6	116.1	95.0	77.0	62.9	52.8	45.8	40.8	36.5
t_d, ºC	194.5	190.3	185.5	179.8	173.4	166.0	157.4	147.2	134.3	115.1	37.8

$$T_s = \begin{cases} 214.48.X^4 - 442.16.X^3 + 208.17.X^2 + 107.07.X + 355.2[K] \ at \ V > 0\, m\, s^{-1} \\ \\ 1000000 \ at \ V < 1 \end{cases} \text{, K} \qquad (38)$$

The function (38) is successfully programmed as additional code in ANSYS CFX to model the boiling of the binary mixture of in the laboratory generator. This determines the boiling temperature in the cells of the element grid

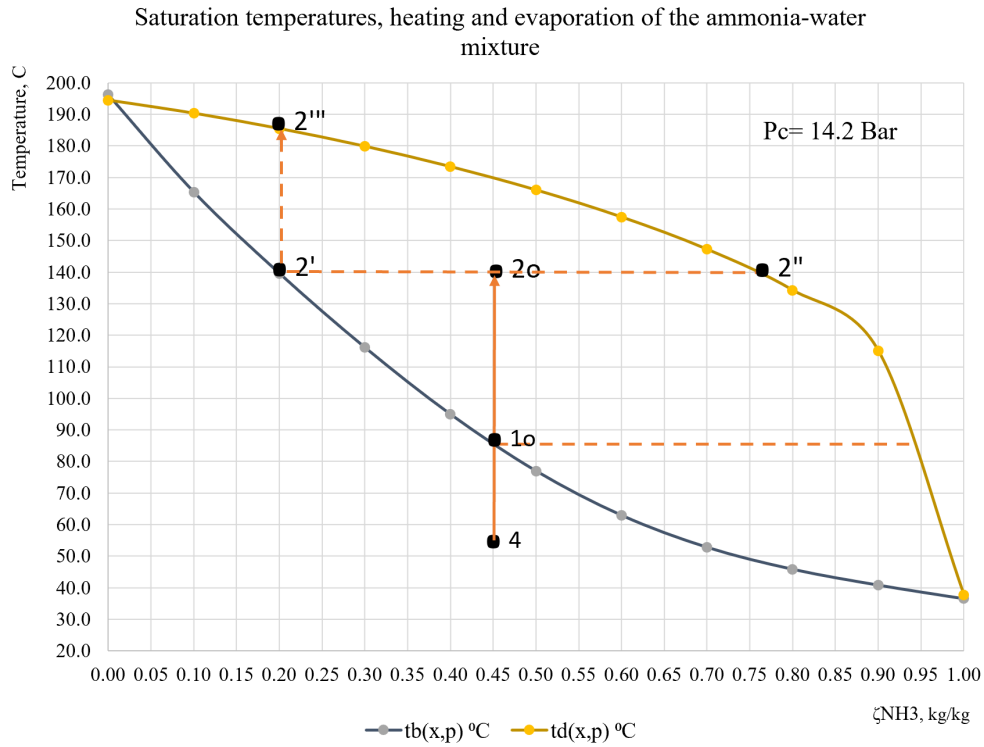


Fig. 4. Heating and boiling of the binary mixture in the laboratory DAR.

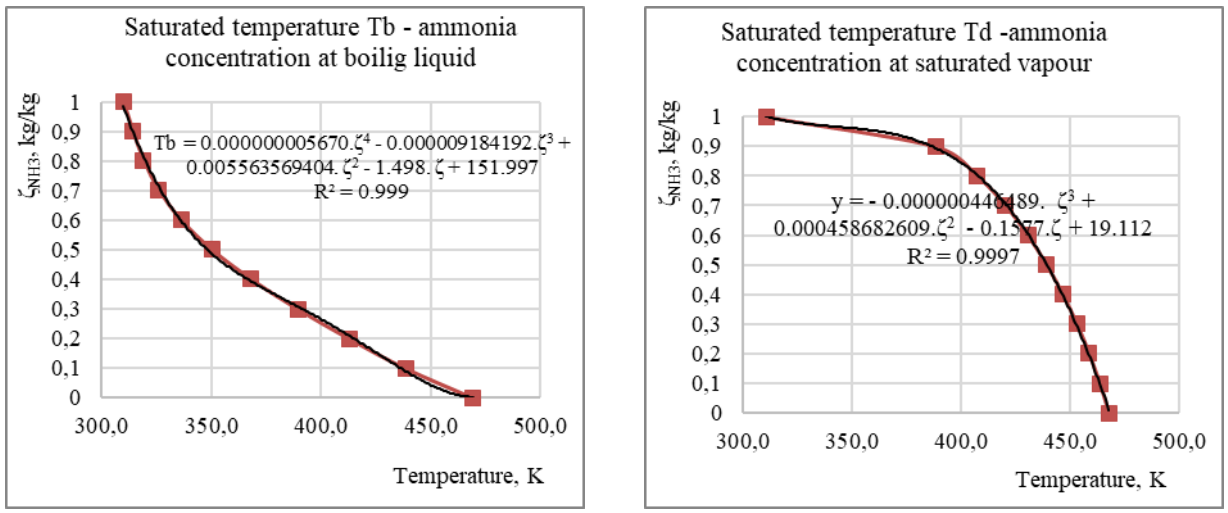


Fig. 5. Variation of the binary mixture saturation temperatures with ammonia concentration.

in which the binary solution is in the wet vapor state. If there is a possibility for boiling of the ammonia-poor solution, recirculating downwards near the thermal contact, a similar polynomial for the dependence of T_s on X at ζ_{rich} = 0.2 (process 2′ - 2‴ in Fig. 4) can be derived and used at the bottom row of Eq. (38).

Table 3. Change of the ammonia concentrations of the wet vapour components and its quality X upon complete evaporation of the liquid.

t_s, ºC	T, K	ζ_{rich}	ζ'	ζ''	X	T, K
83.0	356.2	0.45	0.448	0.96	0.00	356.2
93.0	366.2	0.45	0.398	0.95	0.10	366.2
103.0	376.2	0.45	0.356	0.93	0.16	376.2
113.0	386.2	0.45	0.316	0.90	0.23	386.2
123.0	396.2	0.45	0.276	0.86	0.30	396.2
133.0	406.2	0.45	0.233	0.81	0.38	406.2
143.0	416.2	0.45	0.188	0.74	0.47	416.2
153.0	426.2	0.45	0.140	0.65	0.61	426.2
163.0	436.2	0.45	0.093	0.54	0.80	436.2
170.0	443.2	0.45	0.062	0.45	1.01	443.2

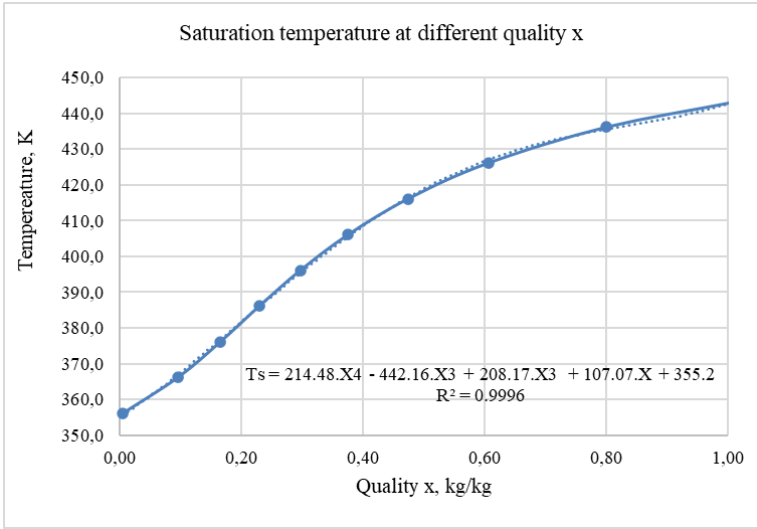


Fig. 6. Function of saturation temperature T_s on the quality X.

CONCLUSIONS

Although modelling and numerical simulation of the boiling of binary mixtures in DAR is a complex task, the advanced software for CFD simulation can applied for this purpose. However, a model of the saturation temperature of the binary solution with the quality of the wet vapour is required. Such a model, convenient for implementation for CFD analyses has been developed and tested in the present study. This allows for the study of different designs and operating generators of DAR and for research and development of the absorption technologies.

Acknowledgements

Authors greatly acknowledge Project КП-06 ПН57/16/ 2021 „Parametric analysis of multiphysical processes in absorption refrigeration systems for efficient utilization of thermal energy“, funded by Bulgarian Ministry of Education and Science, for the assistance of this study.

Authors' contributions

N.P.: conceptions; N.P., Y.S.: mathematical models; K.K., I.K., L.Z., D.D.: experiments; V.I., N.P.: numerical simulations.

REFERENCES

1. B.C. Von Platen, C. G. Munters, Refrigerator U.S. Patent 1685764, 1928.
2. J.L. Rodríguez-Muñoz, J.M. Belman-Flores, Review of diffusion - absorption refrigeration technologies, Renewable and Sustainable Energy Reviews, 30, 2014, 145-153.
3. A. Najjaran, A.A. Harraz, N. Mac Dowell, C.N. Markides, Numerical and experimental investigation of diffusion absorption refrigeration systems for use with low-temperature heat sources, Proc ECOS, 2018, 17-22.
4. B.J.R. Mungyeko Bisulandu, R. Mansouri, A. Ilinca, Diffusion absorption refrigeration systems: An overview of thermal mechanisms and models, Energies, 16, 9, 2023, 3610.
5. S.C.S. Alcântara, J.Â.P. da Costa, A.A.V. Ochoa, G.D.N.P. Leite, Á.A.S. Lima, H.C.N. Silva, P.S.A. Michima, I.C. da Silveira, A.M. de Araújo Caldas, A. Altamirano,. Critical Review of Advances and Numerical Modeling in Absorbers and Desorbers of Absorption Chillers: CFD Applications, Constraints, and Future Prospects, Energies, 18, 2, 2025, 314.
6. R. Garma, Y. Stiriba, M. Bourouis, A. Bellagi, Numerical investigations of the heating distribution effect on the boiling flow in bubble pumps, International Journal of Hydrogen Energy, 39, 27, 2014, 15256-15260.
7. S.W. Jo, S.A. Sherif, W.E. Lear, Numerical simulation of saturated flow boiling heat transfer of ammonia/water mixture in bubble pumps for absorption–diffusion refrigerators, Journal of Thermal Science and Engineering Applications, 6, 1, 201, 2014, 011007.
8. F. Panahizadeh, M. Hamzehei, M. Farzaneh-Gord, A. Antonio Ochoa Villa, Numerical study on heat and mass transfer behavior of pool boiling in LiBr/H_2O absorption chiller generator considering different tube surfaces, Thermal Science, 25, 2B, 2021, 1599.
9. E.Y. Gürbüz, Detailed thermodynamic analysis of the boiler-bubble pump region of a diffusion absorption refrigeration system: experimental and numerical study, Heat and Mass Transfer, 59, 10, 2023, 1837-1853.
10. A. Benhmidene, K. Hidouri, B. Chaouachi, S. Gabsi M. Bourouis, Experimental investigation on the flow behaviour in a bubble pump of diffusion absorption refrigeration systems, Case Studies in Thermal Engineering, 8, 2016. 1-9.
11. Edibon, Practical exercises manual www.edibon.com, 2024, available in August, 2026.
12. Y. Stoyanov, N. Penkova, K. Krumov, Performance of diffusion absorption refrigerators at variable power input, In IOP Conference Series: Earth and Environmental Science Vol. 1380, 1, 2024, 012016.
13. Ansys, Inc., Ansys CFX-Solver Theory Guide (Release 2025 R2), Canonsburg, PA, USA, 2025.
14. N. Kurul, M.Z. Podowski, Multidimensional effects in forced convection subcooled boilin, Proceedings of the 9th International Heat Transfer Conference, 1, 1990, 21-26.
15. J. Patek, J. Klomfar, Simple functions for fast calculations of selected thermodynamic properties of the ammonia-water system., International Journal of Refrigeration, 18, 4, 1995, 228-234
16. R.I. Tanner, J.F. Milthorpe, Numerical simulation of the flow of fluids with yield stress, Numer Meth Lami Turb Flow Seattle, 390, 1983, 680-90.
17. M. Conde-Petit, Thermophysical properties of NH_3-H_2O solutions for the industrial design of absorption refrigeration equipment. Formulation for industrial use, M. Conde Engineering, 2004.
18. T. Todorov, Refrigeration equipment, Techniques Sofia, 1977, (in Bulgarian).
19. T. Todorov, V. Daskalov, Refrigeration exercise manual, Techniques Sofia, 1975, (in Bulgarian).